Journal of Catalysis 340 (2016) 236–247

Contents lists available at ScienceDirect

Journal of Catalysis

journal homepage: www.elsevier.com/locate/jcat

Remarkably efficient CoGa catalyst with uniformly dispersed and trapped structure for ethanol and higher alcohol synthesis from syngas

Xun Ning, Zhe An, Jing He *

State Key Laboratory of Chemical Resource Engineering, Beijing University of Chemical Technology, Beijing 100029, China

ARTICLE INFO

Article history:
Received 31 March 2016
Revised 13 May 2016
Accepted 15 May 2016

Keywords:
Ethanol and higher alcohols
CoGa particles
Syngas transformation
Layered double hydroxides

ABSTRACT

Ethanol and higher alcohols (C_{2+} alcohols) used as liquefaction fuels and/or feedstocks for chemicals could be of great significance if they could be efficiently synthesized from the transformation of biomass-based syngas. Here, we report a uniformly dispersed CoGa catalyst with CoGa particles trapped in the oxide support, which is not only highly active and selective but also distinctively stable in the synthesis of ethanol and higher alcohols from syngas. A 43.5% CO conversion with an alcohol selectivity of 59% has been achieved. In the alcohol products, the fraction of ethanol and higher alcohols reaches 93%. More significantly, the trapped CoGa shows no visible changes of particle dispersion and homogeneous CoGa distribution in the reaction, which gives rise to stable catalytic performance.

1. Introduction

Catalytic conversion of synthesis gas (syngas, CO/H_2) to ethanol and higher (C_{2+}) alcohols has drawn much interest [1–6] owing to the potential use of alcohols as alternative fuels and chemical feedstocks [7–9]. In addition to coal gasification [10,11] and natural gas oxidation [12–14], syngas can be efficiently manufactured from renewable dry biomass [15,16]. The catalytic synthesis of ethanol and higher alcohols from syngas is a reliable method of energy and fuel production independent of fossil resources. The synthesis of C_{2+} alcohols from syngas includes both carbon-chain growth via C–C coupling and alcohol production through CO insertion followed by hydrogenation [17,18]. The kinetic rate match between C–C coupling and CO insertion could promote the production of C_{2+} alcohols, which competes with the formation of methanol and hydrocarbons.

Several catalyst systems have been developed for syngas conversion to ethanol and higher alcohols. Rh is the only single metal able to selectively produce ethanol or C_{2+} oxygenates from CO hydrogenation [19–21]. However, the high cost and limited availability of Rh restrict its large-scale application in syngas conversion. As an alternative, modified Fischer–Tropsch catalysts based on Co and Fe [22–24], as well as Mo-based [25–27] catalysts, have been proposed for C_{2+} alcohol production from syngas. Because Co has prominent chain growth ability [28] and lower activity toward the water–gas shift (WGS) [29,30], Co-based catalysts have been attracting renewed scientific interest. However, a sole Co site has low selectivity toward alcohols because of the deficiency of CO nondissociation sites. One of the approaches is to build bimetallic catalyst systems, such as CoPd [31] or CoCu [32–38]. The selectivity to C_{2+} alcohols is thereby enhanced, as CO adsorption on Pd^0 or Cu^0 is associative rather than dissociative. Moreover, the addition of La_2O_3 dramatically enhances the selectivity to C_{2+} alcohols over Co/AC catalysts [39,40], which is attributed to the generation of Co_2C, which promotes associative Co adsorption [41]. But it is still a great challenge to enhance the selectivity toward C_{2+} alcohols while retaining the activity. Another challenge arises from the poor stability of Co-based catalysts, which generally results from the sintering of the active phase. The agglomeration could also lead to phase separation, which is regarded as the main cause for the decrease in selectivity to alcohols or higher alcohols [42–45]. Except for the report that the copper and cobalt located in the well-defined perovskite structure with a slit-shaped space between nanoparticles improve the stability [46], this remains an issue until now.

Here we report an efficient CoGa catalyst for syngas conversion to ethanol and higher alcohols, in which the CoGa components are uniformly dispersed and the CoGa particles are trapped on the support surface from the in situ transformation of layered double hydroxides (LDHs) (Scheme 1). LDHs, unique two-dimensional nanostructured materials with metal cations distributed in a highly ordered manner in brucite-like layers [47], are an effective precursor for supported metal catalysts with high-density catalytic sites well dispersed [48–51]. The CoGa catalyst prepared in this work displays a selectivity of more than 90% to ethanol and higher alcohols in total alcohol products, with a CO conversion of 43.5%, and especially a stable catalytic performance in the reaction.

* Corresponding author. Fax: +86 10 64425385.
E-mail address: jinghe@263.net.cn (J. He).

http://dx.doi.org/10.1016/j.jcat.2016.05.014
0021-9517/

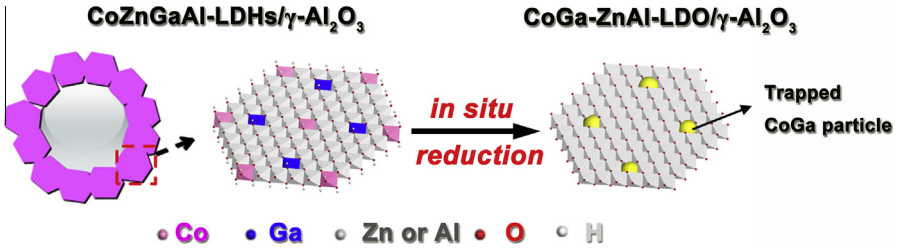

Scheme 1. Schematic illustration for the preparation of uniformly dispersed and trapped CoGa particles from LDHs precursors.

2. Experimental

2.1. Preparation

CoZnGaAl-LDHs with a Co/Ga molar ratio of 5/3 were synthesized in situ on the surface of spherical γ-Al_2O_3 [52], affording a CoZnGaAl-LDHs/γ-Al_2O_3 sample. Typically, 0.0873 g of $Co(NO_3)_2{\cdot}6H_2O$, 0.2678 g of $Zn(NO_3)_2{\cdot}6H_2O$, 0.0345 g of $Ga(NO_3)_3{\cdot}xH_2O$, and 0.2403 g of urea were first dissolved in 1.5 mL of deionized water. The resulting mixed solution was transferred to a 15 mL autoclave. Then 1.0 g of γ-Al_2O_3 (20–40 mesh) was added to the solution as both substrate and Al source. After being kept shaking in a table concentrator for 2 h at room temperature, the autoclave was tightly sealed and maintained at 100 °C for another 12 h. The resulting solid was washed thoroughly with deionized water and then dried at 60 °C for 12 h. CoZnAl-LDHs/γ-Al_2O_3, ZnGaAl-LDHs/γ-Al_2O_3, and ZnAl-LDHs/γ-Al_2O_3 were all synthesized following the same process. The specific surface area of bare γ-Al_2O_3 is 150.3 m^2/g, and the specific surface areas for CoZnGaAl-LDHs/γ-Al_2O_3, CoZnAl-LDHs/γ-Al_2O_3, ZnGaAl-LDHs/γ-Al_2O_3, and ZnAl-LDHs/γ-Al_2O_3 are 186.1 m^2/g, 175.4 m^2/g, 180.7 m^2/g, and 165.3 m^2/g, respectively.

For controls, Co^{2+}/ZnGaAl-LDHs/γ-Al_2O_3 and $Co^{2+}Ga^{3+}$/ZnAl-LDHs/γ-Al_2O_3 with a Co/Ga molar ratio of 5/3 were prepared using the incipient wetness impregnation method. The as-synthesized ZnGaAl-LDHs/γ-Al_2O_3 or ZnAl-LDHs/γ-Al_2O_3 was impregnated with a solution of $Co(NO_3)_2{\cdot}6H_2O$ or a mixed solution of $Co(NO_3)_2{\cdot}6H_2O$ and $Ga(NO_3)_3{\cdot}xH_2O$. After impregnation for 4 h at room temperature, the solid was dried at 100 °C for 12 h.

CoGa–ZnAl-LDO/γ-Al_2O_3 was prepared through in situ reduction of CoZnGaAl-LDHs/γ-Al_2O_3. About 1 g of CoZnGaAl-LDHs/γ-Al_2O_3 was put into a quartz boat, which was placed at the center of a horizontal quartz tube inserted into a furnace at atmospheric pressure. After the removal of air, the furnace was heated under flowing H_2 (40 mL/min) at 5 °C/min to 700 °C. The reduction was maintained for 2 h at 700 °C. After the furnace was cooled to room temperature, 1% O_2–N_2 was introduced into it for another 1 h. The control samples, Co–ZnAl-LDO/γ-Al_2O_3, Co/ZnGaAl-LDO/γ-Al_2O_3, and CoGa/ZnAl-LDO/γ-Al_2O_3, were prepared following the same process by reduction of CoZnAl-LDHs/γ-Al_2O_3, Co^{2+}/ZnGaAl-LDHs/γ-Al_2O_3, and $Co^{2+}Ga^{3+}$/ZnAl-LDHs/γ-Al_2O_3. It should be noted that the catalysts used for characterizations were passivized with pure N_2 instead of 1% O_2–N_2 after the furnace was cooled to room temperature, and preserved under N_2. The Co and Ga content were

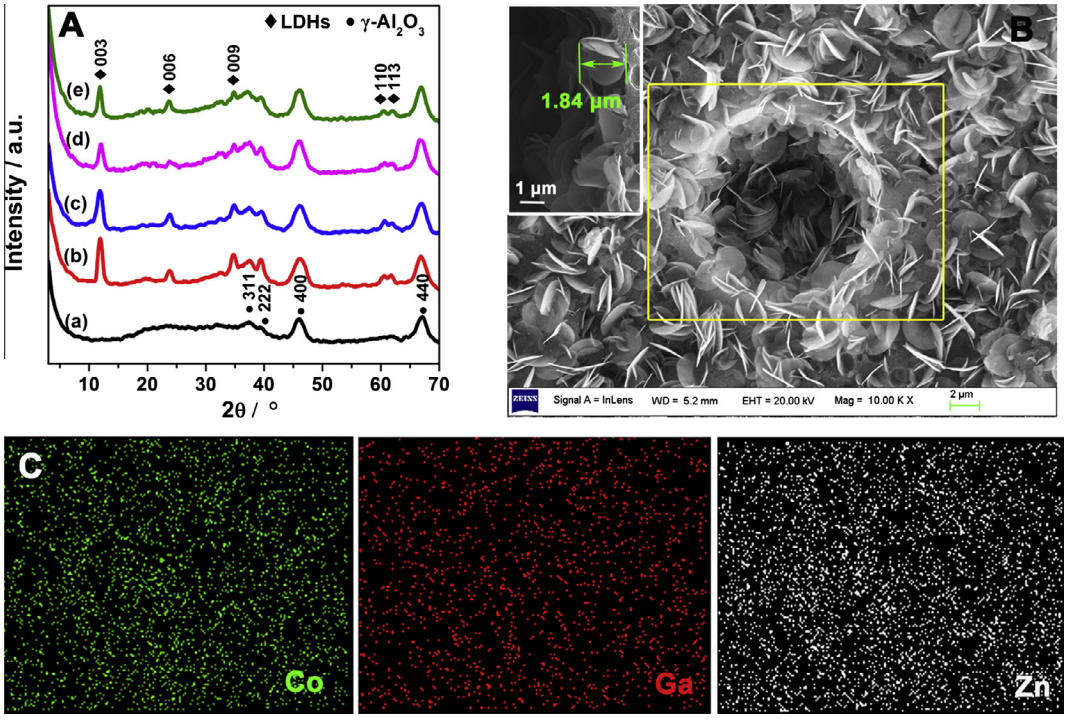

Fig. 1. (A) XRD patterns of (a) γ-Al_2O_3, (b) CoZnGaAl-LDHs/γ-Al_2O_3, (c) CoZnAl-LDHs/γ-Al_2O_3, (d) ZnGaAl-LDHs/γ-Al_2O_3, and (e) ZnAl-LDHs/γ-Al_2O_3. (B) SEM image of CoZnGaAl-LDHs/γ-Al_2O_3 with cross-sectional image inset. (C) SEM–EDS elemental mapping images for Co, Ga, and Zn of the corresponding region (yellow frame in B) of CoZnGaAl-LDHs/γ-Al_2O_3.

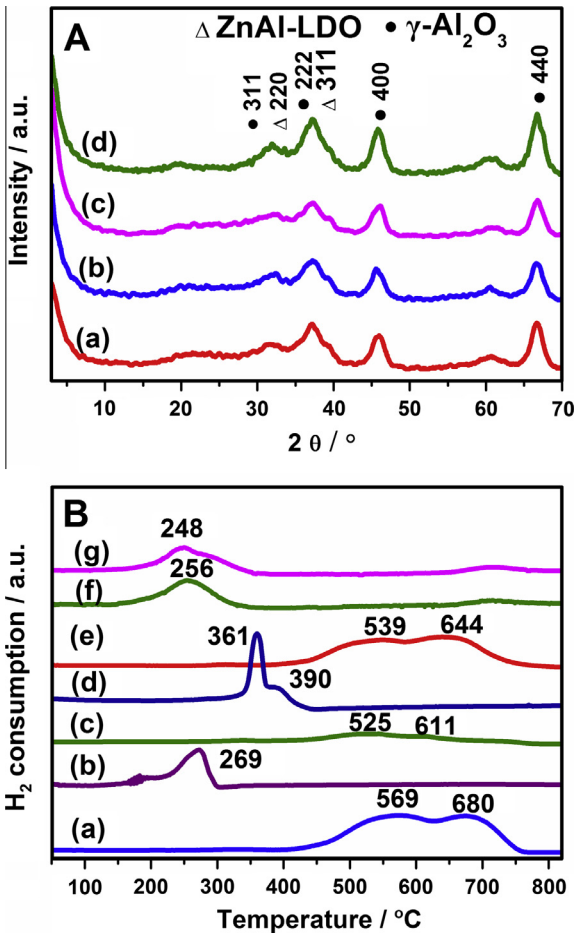

Fig. 2. (A) XRD patterns of (a) CoGa–ZnAl-LDO/γ-Al_2O_3, (b) Co–ZnAl-LDO/γ-Al_2O_3, (c) Co/ZnGaAl-LDO/γ-Al_2O_3, and (d) CoGa/ZnAl-LDO/γ-Al_2O_3. (B) H_2 TPR profiles of (a) CoZnAl-LDHs/γ-Al_2O_3, (b) Co^{2+}/ZnAl-LDHs/γ-Al_2O_3, (c) ZnGaAl-LDHs/γ-Al_2O_3, (d) Ga^{3+}/ZnAl-LDHs/γ-Al_2O_3, (e) CoZnGaAl-LDHs/γ-Al_2O_3, (f) Co^{2+}/ZnGaAl-LDHs/γ-Al_2O_3, and (g) $Co^{2+}Ga^{3+}$/ZnAl-LDHs/γ-Al_2O_3.

determined by ICP-ES as 1.57 and 1.06 wt.% for CoGa–ZnAl-LDO/γ-Al_2O_3, 1.62 and 1.03 wt.% for Co/ZnGaAl-LDO/γ-Al_2O_3, and 1.59 and 1.05 wt.% for CoGa/ZnAl-LDO/γ-Al_2O_3, respectively. The Co content in Co–ZnAl-LDO/γ-Al_2O_3 was determined to be 1.53 wt.%.

2.2. Characterizations

X-ray diffraction (XRD) measurements were carried out on a Shimadzu XRD-6000 powder diffractometer with Cu Kα radiation (λ = 0.154 nm) operated at 40 kV and 30 mA. The XRD patterns for all the samples were collected with a scanning angle (2θ) range of 3–70° at a scanning rate of 5°/min. The quantitative elemental analysis for Co and Ga was performed using a Shimadzu ICPS-75000 inductively coupled plasma emission spectrometer (ICP-ES). N_2 adsorption/desorption experiments were carried out on a Quantachrome Autosorb-1 system. The specific surface area was determined by Brunauer–Emmett–Teller (BET) methods using a Quantachrome Autosorb-1C-VP analyzer. The samples were outgassed in N_2 flow at 120 °C for 2 h prior to measurement. The SEM images were taken on a Zeiss Supra 55 scanning electron microscope equipped with an energy-dispersive spectrum (EDS) attachment. TEM and HRTEM images were taken on a Tecnai G2 F20 S-TWIN operated at 300 kV. High-angle annular dark field (HAADF) images and elemental analysis (mapping and line scan) were taken in STEM mode. The samples for STEM measurements were treated in ethanol under ultrasonic conditions before deposition on a Cu microgrid and covered with a carbon coating of several nanometers to eventually prevent magnetization. The temperature-programmed reduction (H_2 TPR) of the catalyst precursor was performed on a Micrometric ChemiSorb 2720 chemisorption system with a thermal conductivity detector (TCD). The sample (~0.1 g) was pretreated in a flow of Ar (40 mL/min) at 150 °C for 1 h to remove the water and then cooled to 30 °C. An H_2 TPR profile was recorded from 30 to 900 °C at a heating rate of 10 °C/min in a flow of 10% H_2–Ar (40 mL/min). The temperature-programmed desorption of H_2 (H_2 TPD) on each catalyst was carried out on the same equipment. The sample (~0.1 g) was pretreated in a flow of 10% H_2–Ar (40 mL/min) at 400 °C for 1 h, cooled to 100 °C, held at 100 °C for 1 h for H_2 absorption, and then purged by a flow of Ar (40 mL/min). The H_2 TPD profile was recorded from 100 to 450 °C at a heating rate of 10 °C/min and held at 450 °C for 2 h in a flow of Ar (40 mL/min). Calculations for Co dispersion were made using the total amount of adsorbed hydrogen and a stoichiometry of one hydrogen atom per cobalt surface atom. The dispersion was also determined from TEM images by the particle mean size, assuming a surface atom density of 14.6 Co atoms/nm^2 [53]. The Co *K*-edge X-ray absorption near-edge structure (XANES) spectra were recorded in transmission mode at room temperature at beam line 1W1B of at the Beijing Synchrotron Radiation Facility (BSRF), Institute of High Energy Physics, Chinese Academy of Science. A Si (III) double crystal was used to monochromatize the X-rays from the 700 MeV electron storage ring. XANES data were examined by Athena program.

2.3. Catalytic test

The catalytic test was performed in a stainless steel fixed-bed reactor. A portion of 0.6 g of catalyst (20–40 mesh) was loaded into the reactor. The remaining volume of the reactor tube was filled with quartz beads of 20–40 mesh. Prior to the reaction, the catalyst was activated in situ with H_2 at atmospheric pressure with a flow rate of 2000 h^{-1} at 40 °C for 1 h. After the reactor was cooled to 50 °C, the reactor was heated to the reaction temperature with a ramp rate of 2 °C/min and a syngas (H_2/CO = 2.0, 5% argon as internal standard) flow rate of 2000 h^{-1}. When the reaction temperature was reached, the system was pressurized to 3.0 MPa with syngas. The reaction was conducted at 240, 260, 280, and 300 °C.

After passing through a hot trap (180 °C) and a cold trap (0 °C), the tail gas was analyzed online by GC. Ar, CO, CH_4, and CO_2 were analyzed through a TDX-1 packed column with a thermal conductivity detector (TCD), using He as carrier gas (Fig. S1 in the Supplementary Information). C_1–C_5 hydrocarbons were analyzed through an Al_2O_3 packed column with N_2 carrier and hydrogen flame ionization detector (FID) (Fig. S2). The aqueous and oil liquid products (Table S1), collected from the cold trap and hot trap, were analyzed offline by GC. The aqueous products containing alcohols mostly were analyzed through GSBP-INOWAX (30 m × 0.25 mm × 0.5 μm) with an N_2 carrier and FID. Sec-butyl alcohol was used as an internal standard (Fig. S3). The liquid oil products were diluted in cyclohexane solvent and analyzed through a DB-5 column with N_2 carrier and FID. Ethyl cyclohexane was used as an internal standard (Fig. S4). CO conversion (χ_{CO}) and selectivity of products were calculated according to the following equations:

$$\chi_{CO} = \frac{F_{CO_{in}} - F_{CO_{out}}}{F_{CO_{in}}} \times 100\%$$

$$S_{C_i} = \frac{F_{C_i} \times i}{F_{CO_{in}} - F_{CO_{out}}} \times 100\%$$

$$S_{ROH} = \sum_{i=1}^{n} S_{C_iH_{2i}OH},$$

where F is the moles of CO and product C_i (CO_2, hydrocarbon or alcohols) containing i carbon atoms. The mass balance and carbon

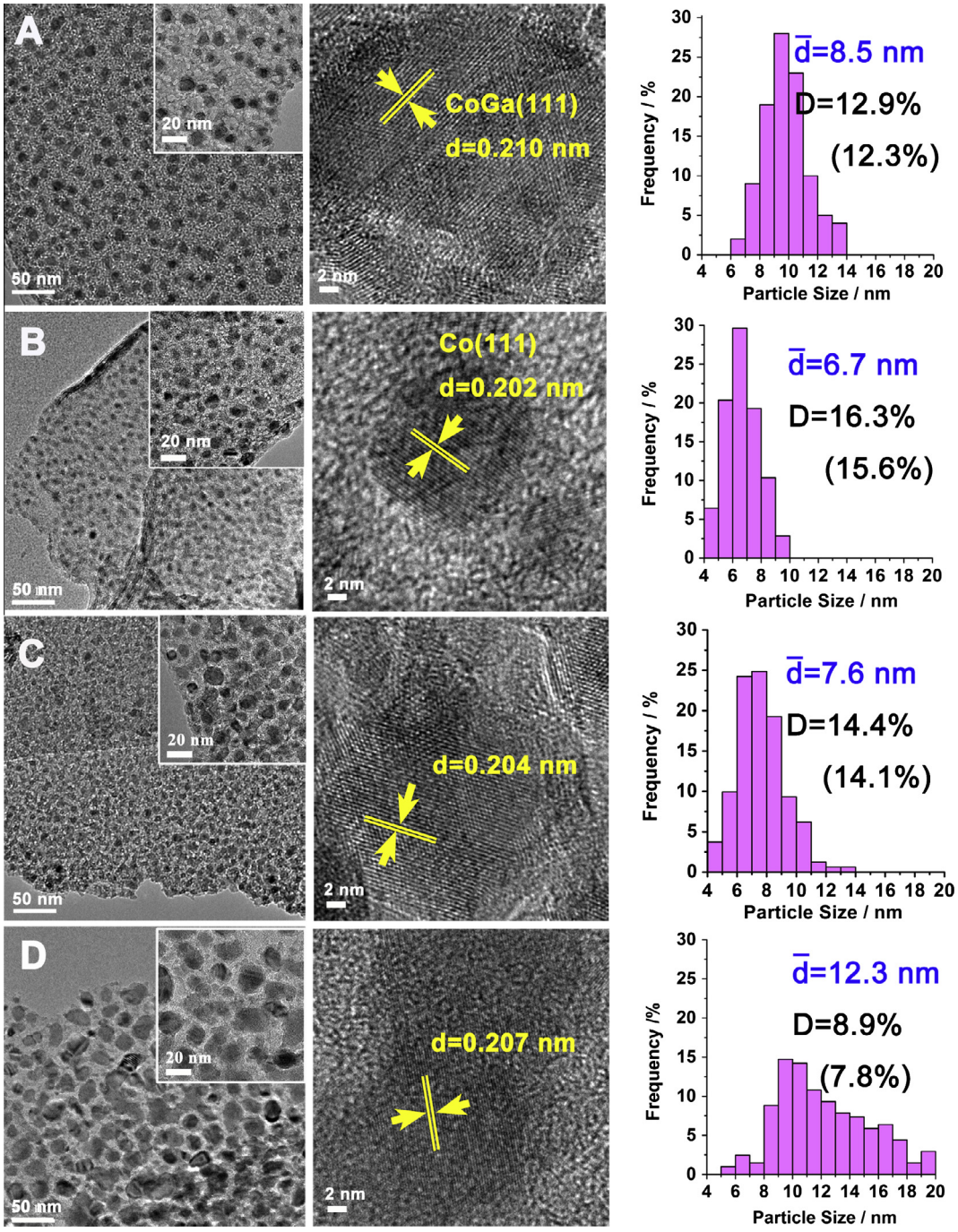

Fig. 3. TEM images, HRTEM images, and particle size distributions for (A) CoGa–ZnAl-LDO/γ-Al_2O_3, (B) Co–ZnGaAl-LDO/γ-Al_2O_3, (C) Co/ZnGaAl-LDO/γ-Al_2O_3, and (D) CoGa/ZnAl-LDO/γ-Al_2O_3. The estimated mean sizes and dispersions (*D*) are given with the particle size distributions. The particle size distributions and mean sizes were based on 250 particles counted in various regions. The dispersions were determined by the particle mean sizes assuming a surface atom density of 14.6 Co atoms/nm^2 [53]. The dispersions determined by H_2 chemisorption are shown in parentheses.

balance have been calculated at each product and kept between 90% and 95%.

3. Results and discussion

3.1. Supported CoGa catalysts

3.1.1. Dispersion of CoGa particles

CoZnGaAl-LDHs with a Co/Ga molar ratio of 5/3, as the precursor for preparation of CoGa supported on ZnAl-LDO, were synthesised in situ on the γ-Al_2O_3 support using urea as the precipitant [52]. For comparison, CoZnAl-LDHs, ZnGaAl-LDHs, and ZnAl-LDHs were also synthesized on γ-Al_2O_3 as well. In the X-ray diffraction (XRD) patterns (Fig. 1A), in addition to the reflections characteristic of γ-Al_2O_3 at 37.42°, 39.25°, 45.84°, and 67.08° (JCPDS: 10-0425), the (003), (006), (009), (110), and (113) reflections at about 11.7°, 23.6°, 35.4°, 60.3°, and 61.2° characteristic of a hydrotalcite-like structure are clearly observed in each LDH-grown sample. The basal spacing is estimated to be nearly 0.73 nm, illustrating that the interlayer anion is CO_3^{2-}. The lattice parameter *a* (*a* = 2*d*(110)) for CoZnGaAl-LDHs (*a* = 1.5288) is larger than that for CoZnAl-LDHs (*a* = 1.5268), resulting from the greater

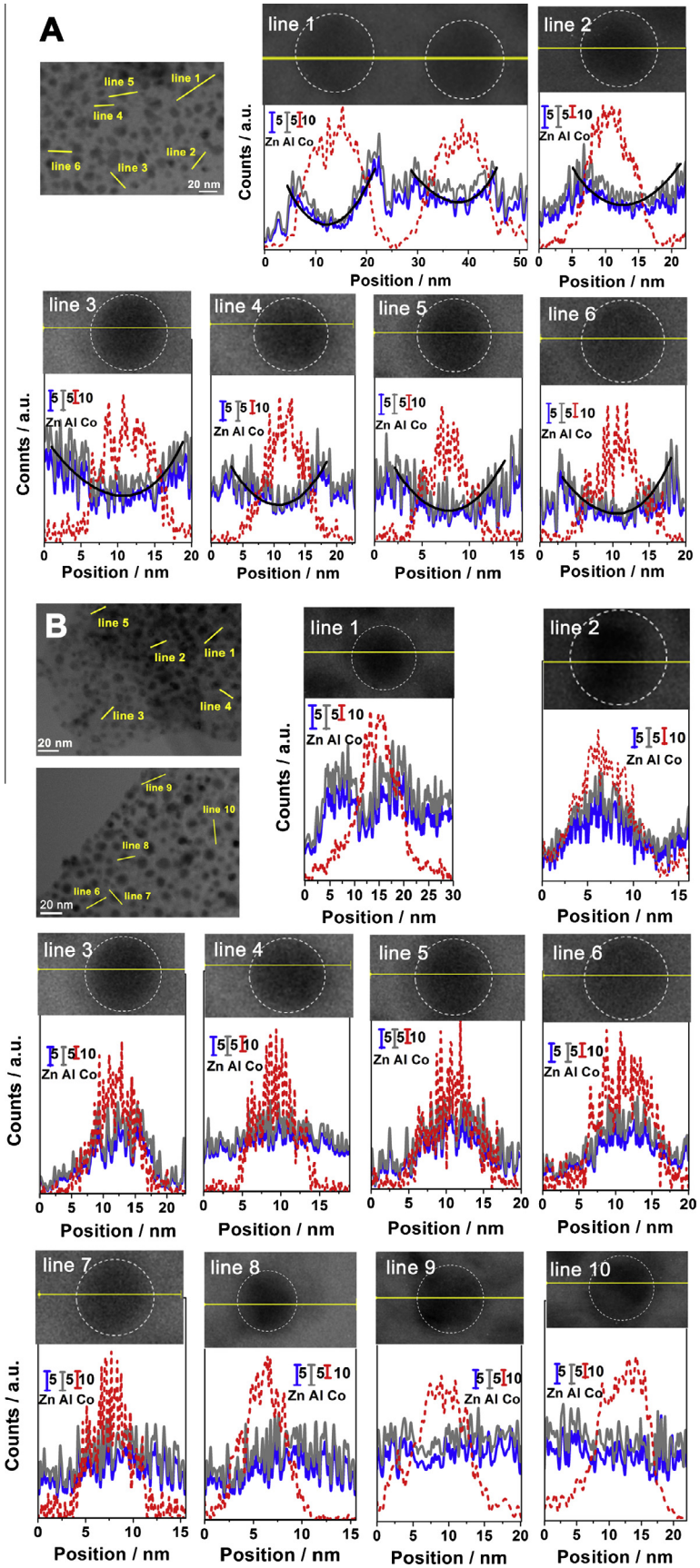

Fig. 4. Line scan profiles of Zn and Al population (full lines) and Co population (dashed lines) in (A) CoGa–ZnAl-LDO/γ-Al_2O_3 and (B) Co/ZnGaAl-LDO/γ-Al_2O_3 to show the stabilization of CoGa particles anchored by the traps in the LDO supports transformed CoZnGaAl-LDHs.

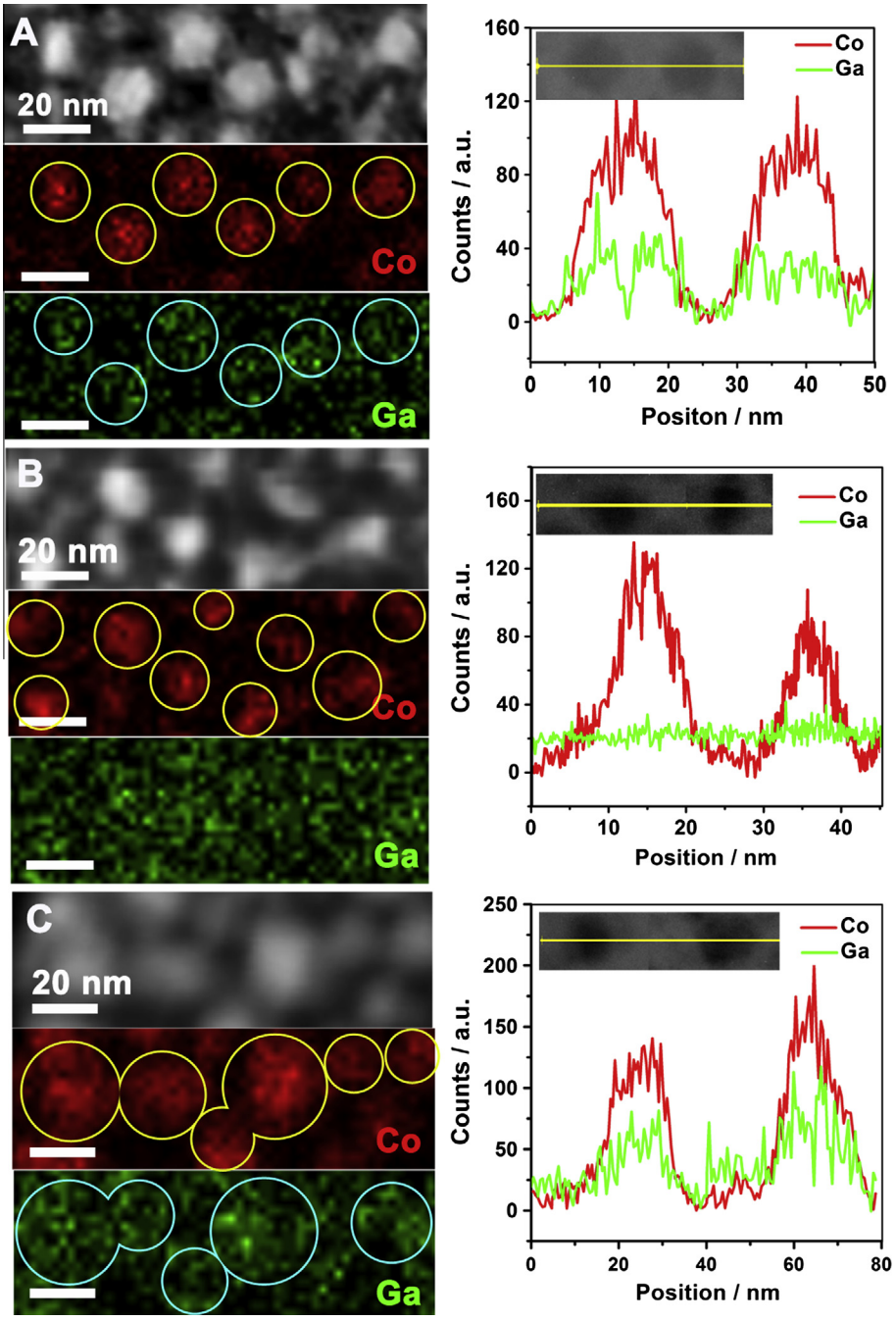

Fig. 5. HAADF images with Co (red) and Ga (green) element mapping and linescan profiles along the yellow line for (A) CoGa–ZnAl-LDO/γ-Al_2O_3, (B) Co/ZnGaAl-LDO/γ-Al_2O_3, and (C) CoGa/ZnAl-LDO/γ-Al_2O_3.

Ga–O length (1.92 Å) than Al–O length (1.91 Å). A similar expansion of the lattice parameter *a* is also observed for ZnGaAl-LDHs (*a* = 1.5249) by comparison with ZnAl-LDHs (*a* = 1.5224), which proves the substitution of Ga^{3+} for Al^{3+} in the LDH brucite-like layers. From the SEM images (Fig. 1B), the CoZnGaAl-LDHs are grown densely on both exterior and interior surfaces of γ-Al_2O_3, displaying a thickness of approximately 1.84 μm. The SEM–EDS element mapping images (Fig. 1C) offer clear evidence for the homogeneous distribution of Co, Ga, and Zn elements in the LDH layers. In comparison with bare γ-Al_2O_3, all the LDH-grown samples exhibit increased specific surface area due to the orientation growth of LDHs on the γ-Al_2O_3 support.

After thermal treatment of CoGa–ZnAl-LDHs/γ-Al_2O_3 or Co–ZnAl-LDHs/γ-Al_2O_3 at 700 °C under H_2 for 2 h, CoGa–ZnAl-LDO/γ-Al_2O_3 or Co–ZnAl-LDO/γ-Al_2O_3 was produced. For comparison, Co/ZnGaAl-LDO/γ-Al_2O_3 and CoGa/ZnAl-LDO/γ-Al_2O_3 with Co and/or Ga loadings similar to those on CoGa–ZnAl-LDO/γ-Al_2O_3 were prepared by thermally treating Co/ZnGaAl-LDHs/γ-Al_2O_3 and CoGa/ZnAl-LDHs/γ-Al_2O_3 at 700 °C under H_2 for 2 h, in which the Co/ZnGaAl-LDHs/γ-Al_2O_3 or CoGa/ZnAl-LDHs/γ-Al_2O_3 was prepared by impregnation of ZnGaAl-LDHs/γ-Al_2O_3 or ZnAl-LDHs/γ-Al_2O_3 with Co^{2+} or Co^{2+}/Ga^{3+} salts. In the XRD patterns (Fig. 2A), in addition to the reflections of γ-Al_2O_3, the ZnAl-LDO phase can be clearly seen in each reduced sample according

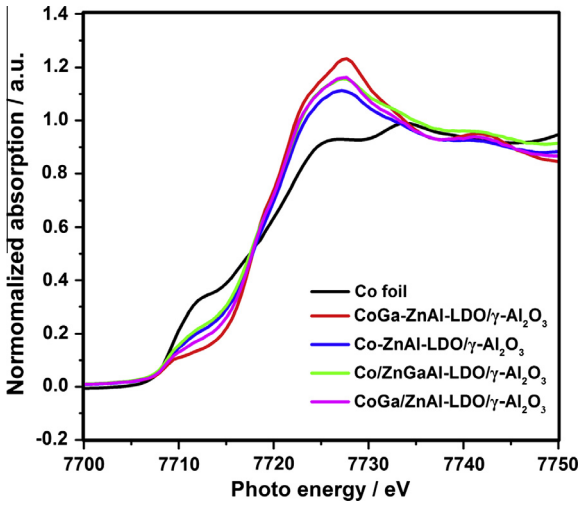

Fig. 6. The normalized intensity of Co *K*-edge XANES spectra of Co foil, CoGa–ZnAl-LDO/γ-Al_2O_3, Co–ZnAl-LDO/γ-Al_2O_3, Co/ZnGaAl-LDO/γ-Al_2O_3, and CoGa/ZnAl-LD O/γ-Al_2O_3.

to the reflections at 32.17° and 37.52° (JCPDS: 05-0669). The diffractions attributed to Co or CoGa (Co JCPDS: 15-0806, 2θ(111) = 44.2°, d(111) = 0.202 nm; CoGa JCPDS: 15-0578, 2θ(111) = 42.8°, d(111) = 0.210 nm) are difficult to identify because they are close to those of the (400) reflection of γ-Al_2O_3, or the metal phase exists in a highly uniform dispersion. The presence of Co or CoGa is revealed from the H_2 TPR of the catalyst precursor. As shown in Fig. 2B, the H_2 consumptions are observed at 569 and 680 °C for CoZnAl-LDHs/γ-Al_2O_3 and at 525 and 611 °C for ZnGaAl-LDHs/γ-Al_2O_3. The H_2 consumption between 500 and 700 °C is attributed to the reduction of Co(II) to Co^0 [54] and Ga (III) to Ga^0 [55]. Notably, the temperatures of H_2 consumption for CoZnAl-LDHs/γ-Al_2O_3 or ZnGaAl-LDHs/γ-Al_2O_3 are much higher than those for Co^{2+}/ZnAl-LDHs/γ-Al_2O_3 (269 °C) or Ga^{3+}/ZnAl-LDHs/γ-Al_2O_3 (361 and 390 °C), indicating that the reduction of Co(II) or Ga(III) confined in the LDH layers is more difficult. In comparison with CoZnAl-LDHs/γ-Al_2O_3, the temperatures of H_2 consumption for CoGaZnAl-LDHs/γ-Al_2O_3 decrease by 30 °C. This is indicative of an interaction between Co and Ga, revealing the formation of CoGa particles. For Co^{2+}/ZnGaAl-LDHs/γ-Al_2O_3 or $Co^{2+}Ga^{3+}$/ZnAl-LDHs/γ-Al_2O_3, the temperature of H_2 consumption decreases by 13 or 21 °C, suggesting the weakened Co–Ga interaction.

Visible particles can be observed in the TEM images (Fig. 3). From the HRTEM image of CoGa–ZnAl-LDO/γ-Al_2O_3 (Fig. 3A), the (111) facet assigned to CoGa particles can be clearly observed, with a lattice spacing of 0.210 nm. The CoGa particles exhibit extraordinarily excellent dispersion with a narrow size distribution from 6 to 14 nm and a mean size of 8.5 nm. The dispersion is 12.9% (12.3%). For Co–ZnAl-LDO/γ-Al_2O_3 (Fig. 3B), the HRTEM image shows the (111) facet of Co particles, with a lattice spacing of 0.202 nm. The particle size ranges between 3 and 10 nm (mean size = 6.7 nm) and the dispersion is 16.3% (15.6%). However, in Co/ZnGaAl-LDHs/γ-Al_2O_3, which is produced from ZnGaAl-LDHs with Co salts impregnated, the lattice spacing of the (111) facet is estimated to be 0.204 nm (Fig. 3C). The particle size ranges from 4 to 12 nm (mean size = 7.6 nm) and the dispersion is 14.4% (14.1%). For CoGa/ZnAl-LDO/γ-Al_2O_3 (Fig. 3D), which is produced from the ZnAl-LDHs with both Co and Ga salts impregnated, the particle size ranges from 5 to 20 nm (mean size = 12.3 nm) and the dispersion is 8.9% (7.8%). The lattice spacing of the (111) facet is estimated to be 0.207 nm, similar to that for CoGa particles. Therefore, the insertion of Co and/or Ga cations into the lattices of LDH layers facilitates Co or CoGa particles with small size and narrow size distribution. It is obvious that the lattice spacing increases in the order Co–ZnAl-LDO/γ-Al_2O_3 < Co/ZnGaAl-LDO/γ-Al_2O_3 < CoGa/ZnAl-LDO/γ-Al_2O_3 < CoGa–ZnAl-LDO/γ-Al_2O_3, which visibly depends on whether and how Ga has been introduced. The difference in the lattice spacing might be relevant to the Co and Ga distribution, which is to be discussed hereafter.

3.1.2. Trapped accommodation of CoGa particles

From the TEM images (Fig. 3A) of CoGa–ZnAl-LDO/γ-Al_2O_3, the CoGa particles are clearly observed to be trapped in the ZnAl-LDO. To confirm the trapped structure, Zn and Al populations in the LDO support are counted. As shown in Fig. 4A, the scanned Zn and Al populations corresponding to the inset TEM image shows a periodic decrease/increase, and the decrease position exactly matches the presence of CoGa particles. In virtue of the unique structure of LDH materials, the elements Co, Ga, Zn, and Al are all distributed in a highly ordered manner in the LDH layers. During the topological transformation/in situ reduction of LDHs to LDOs and metal particles, Co and Ga are reduced to form CoGa particles and Zn and Al are transformed to oxides. The traps for the metal particles are generated where Zn and Al are absent. Obviously, the observed traps accommodate the CaGa particles, which can be expected to suppress the migration and aggregation of CoGa particles effectively. For Co/ZnGaAl-LDO/γ-Al_2O_3, which is produced from the Co-salt-impregnated ZnGaAl-LDHs, the decrease/increase of Zn and Al populations is not always visible, and the positions of population decrease (traps) are not observed to accommodate the CoGa particles (Fig. 4B). The elements Zn, Ga, and Al are all

Table 1
Catalytic performance of CoGa–ZnAl-LDO/γ-Al_2O_3, Co–ZnAl-LDO/γ-Al_2O_3, Co/ZnGaAl-LDO/γ-Al_2O_3, and CoGa/ZnAl-LDO/γ-Al_2O_3 for synthesis of ethanol and higher alcohols from syngas.[a]

Catalyst	Reaction time (h)	TOF (10^{-3} s^{-1})[b]	CO conversion (%)	Selectivity (C mol%)[c]				Alcohols distribution (wt.%)[d]				
				CH_4	$C_{2+}H$	ROH	CO_2	MeOH	EtOH	PrOH	BuOH	$C_{5+}OH$
CoGa–ZnAl-LDO/γ-Al_2O_3	15	37.9	43.5	10.9	29.0	59.0	1.2	7.2	30.8	14.3	10.1	37.7
	2		15.8	9.5	24.6	64.6	3.9	6.7	25.6	12.9	9.8	45.0
	3.3		27.3	8.9	27.6	61.0	2.5	6.7	29.9	14.3	9.6	39.5
	4.7		32.9	9.7	28.3	59.8	2.2	7.6	29.8	13.4	10.0	39.2
Co–ZnAl-LDO/γ-Al_2O_3	15	29.4	27.0	14.1	54.4	29.6	1.9	24.6	28.5	12.6	9.2	25.1
Co/ZnGaAl-LDO/γ-Al_2O_3	15	31.8	32.5	14.8	32.7	50.5	2.0	13.8	40.4	12.8	11.8	21.2
CoGa/ZnAl-LDO/γ-Al_2O_3	15	34.2	15.4	13.8	33.2	51.6	1.4	12.7	24.0	11.1	10.7	41.4

[a] Reaction conditions: T = 260 °C, P = 3 MPa, $n(H_2)/n(CO)$ = 2.0, GSHV = 2000 h^{-1}.
[b] TOF values are based on the dispersion estimated from the TEM images.
[c] Carbon selectivity is defined as the selectivity of all the carbon-containing products from converted carbon; $C_{2+}H$ = hydrocarbons exclusive of methane; ROH = total 1-alcohols.
[d] Alcohol distribution (wt.%): the weight fraction of each alcohol in the total alcohols.

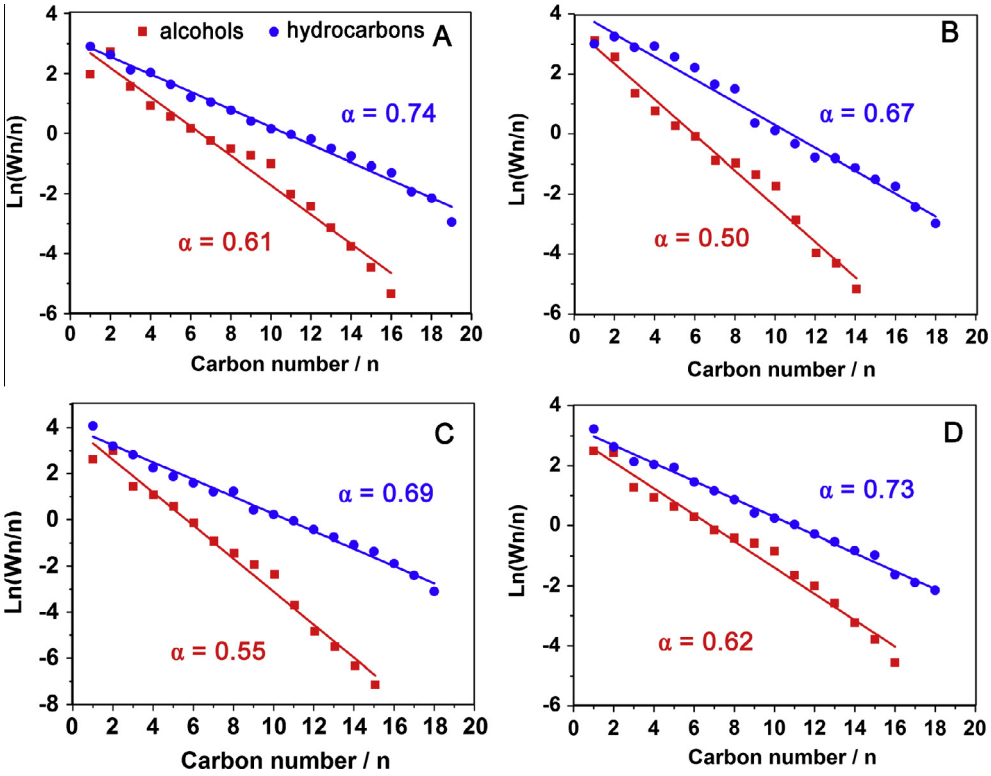

Fig. 7. Anderson–Schulz–Flory (A–S–F) plots for the distribution of alcohols and hydrocarbons obtained at 15 h reaction for (A) CoGa–ZnAl-LDO/γ-Al_2O_3, (B) Co–ZnAl-LDO/γ-Al_2O_3, (C) Co/ZnGaAl-LDO/γ-Al_2O_3, and (D) CoGa/ZnAl-LDO/γ-Al_2O_3. The A–S–F chain growth probability α of products is calculated according to the equation $\ln(W_n/n) = n \ln\alpha + \ln(1-\alpha)^2/\alpha$, in which n is the number of carbon atoms in products, W_n is the weight fraction of products containing n carbon atoms, and $1-\alpha$ is the probability of chain termination. The α-values are based on the confidence level over 96%.

Table 2
CO conversion and alcohol selectivity in some representative catalysts reported in references.

Catalysts	T (°C)	H_2/CO[a]	P (MPa)	GHSV (h^{-1})	CO conversion (%)	S_{ROH} (%)	S_{C2+OH} (%)
CoGa–ZnAl-LDO/γ-Al_2O_3[b]	260	2	3	2000	43.5	59.0	92.8
Cu–Co/ZrO_2 [42]	310	2	4.5	3900	60	55	NA
Cu@(CuCo-alloy)/Al_2O_3 [37]	220	2	2	2000[c]	21.5	50.6	80.8
Co–Co_2C/AC1 [41]	220	2	3	33.6[d]	71.4	38.4	92.6
3DOM Cu2Fe1 [24]	200	1	6	2000	12.9	47.6	94.6
$Co_1Cu_1Mn_1$ [35]	240	2	6	2000	18	37.5	NA
20%Cu–Co/La_2O_3–SiO_2 [59]	330	2	3	3900[c]	32.1	39.5	66.1
15Cu5Co/Al_2O_3 [34]	250	2	2	1800[c]	23.2	23.3	79.3

[a] The mole ratio of H_2 to CO.
[b] Catalyst in this work.
[c] The unit is mL $(g_{cat}h)^{-1}$.
[d] The unit is mL/min.

distributed in a highly ordered manner in the LDH layers. In the reduction of LDHs without reducible metal cations in the layers, only –OHs are removed to make a rough surface. The generated pits on the surface of ZnGaAl-LDO are too small to accommodate the particles in nanoscale. The results offer evidence for the trapped CoGa particles in CoGa–ZnAl-LDO/γ-Al_2O_3, which is due to the confinement of CoGaZnAl-LDHs structure in the calcination/reduction from CoZnGaAl-LDHs.

3.1.3. Distribution of Co and Ga

The distribution of Co and Ga in CoGa–ZnGa-LDO/γ-Al_2O_3, Co/ZnGaAl-LDO/γ-Al_2O_3, and CoGa/ZnAl-LDO/γ-Al_2O_3 was measured by EDS element mapping and linescan technique (Fig. 5). For CoGa–ZnGa-LDO/γ-Al_2O_3 derived from CoZnGaAl-LDHs/γ-Al_2O_3, both Co and Ga islands are observed, with Ga overlapped with Co, which indicates a contiguous distribution of Co and Ga (Fig. 5A). But in Co/ZnGaAl-LDO/γ-Al_2O_3, the Ga is observed to be in a homogeneous and continuous distribution, while the Co is visibly distributed in islands (Fig. 5B). The inhomogeneous distribution of Co and Ga results in a (111) lattice of particles in Co/ZnGaAl-LDO/γ-Al_2O_3 similar to that of the Co particles in Co–ZnAl-LDO/γ-Al_2O_3. Co and Ga distributed in islands are also observed in CoGa/ZnAl-LDO/γ-Al_2O_3 (Fig. 5C), but less homogeneous than for the CoGa–ZnAl-LDO/γ-Al_2O_3 produced from CoGaZnAl-LDHs/γ-Al_2O_3 with both Co and Ga located in the LDH brucite-like lattices. Therefore, introducing Co and Ga in the same way helps promote their contiguous distribution to form a CoGa phase. By using CoGaZnAl-LDHs/γ-Al_2O_3 as precursor, in which Co and Ga cations are both introduced into the lattices of LDHs in the formation of the LDH precursor, well-defined CoGa particles

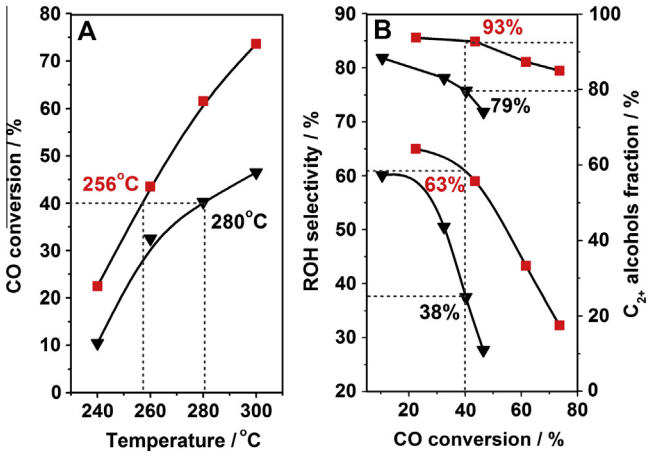

Fig. 8. (A) Profiles of CO conversion as a function of reaction temperature and (B) alcohol selectivity and C_{2+} alcohol selectivity as functions of CO conversion on CoGa–ZnAl-LDO/γ-A_2O_3 (square symbols) and Co/ZnGaAl-LDO/γ-A_2O_3 (triangle symbols).

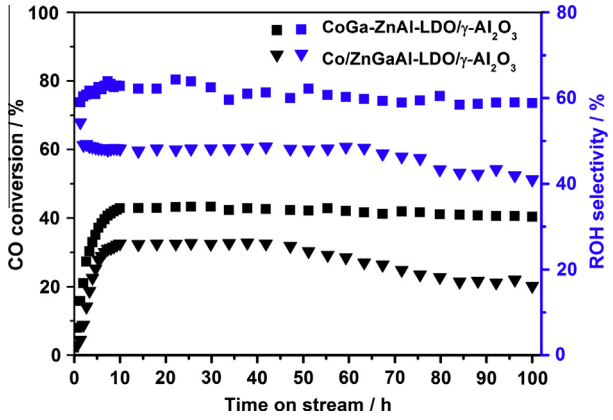

Fig. 9. CO conversion and ROH selectivity with reaction time on stream (100 h) on CoGa–ZnAl-LDO/γ-A_2O_3 (square symbols) and Co/ZnGaAl-LDO/γ-A_2O_3 (triangle symbols). The reaction was carried out at T = 260 °C, P = 3 MPa, GHSV = 2000 h^{-1}, n(H_2)/n(CO) = 2.0.

with a narrow size distribution have been produced. The well-defined CoGa particles from CoGaZnAl-LDHs/γ-Al_2O_3 are further confirmed by XANES results (Fig. 6), in which the photoenergy reflects the electronic structure of the Co center. The lowest energy of the Co *K*-edge is detected in CoGa–ZnAl-LDO/γ-Al_2O_3, indicative of the greatest enrichment of electrons on the Co atom. This illustrates that the Co sites in CoGa–ZnAl-LDO/γ-Al_2O_3 tend to be more negative, as the intimate contact of Co and Ga in the well-defined CoGa particles facilitates electron transfer from Ga (electronegativity 1.6) to Co (electronegativity 1.88).

3.2. Syngas to ethanol and higher alcohols

CoGa–ZnAl-LDO/γ-A_2O_3 was then used as the catalyst for conversion of syngas to ethanol and higher alcohols. For comparison, catalysis by Co–ZnAl-LDO/γ-A_2O_3, Co/ZnGaAl-LDO/γ-A_2O_3, and CoGa/ZnAl-LDO/γ-A_2O_3 has also been evaluated. The comparison is made in terms of CO conversion, selectivity, and A nderson–Schulz–Flory (A–S–F) α-chain-growth probability (Table 1). To allow the selectivity comparison, the catalytic results on CoGa–ZnAl-LDO/γ-A_2O_3 are provided at varied CO conversions. CoGa–ZnAl-LDO/γ-A_2O_3 exhibits higher CO conversion and C_{2+} alcohol selectivity than the other three catalysts. CO conversion on CoGa–ZnAl-LDO/γ-A_2O_3 reaches 43.5% at 15 h, with an alcohol selectivity of 59%. Among the alcohol products, the fraction of ethanol and higher alcohols is up to 92.8%. According to GC–MS analysis results (see the Supplementary Information), the alcohol products are composed of 1-alcohols with the carbon number ranging up to C_{16}. As expected, unwanted CO_2 is under control for all the four catalysts.

Mass transport and heat transfer calculations were performed for CoGa–ZnAl-LDO/γ-A_2O_3 with 43.5% CO conversion, using Weisz–Prater and Mears analyses [56,57] (see the Supplementary Information). The Weisz–Prater criterion,

$$C_{WP} = \frac{-r'_{A(obs)}\rho_c R^2}{D_e C_{As}} < 1,$$

gives $2.72 \times 10^{-3} < 1$, indicative of no internal diffusion limitations. The Mears criterion,

$$\frac{-r'_A R^2}{C_{Ab} D_e} < \frac{1 + 0.33\gamma\chi}{|n - \gamma_b\beta_b|(1 + 0.33n\omega)},$$

gives $3.17 \times 10^{-6} < 1.0$, indicating no interphase and intraparticle heat transfer or mass transport limitations. Thus our catalytic system is free from mass transport and heat transfer limitations.

3.2.1. Improved catalysis of well-distributed CoGa

As can be seen from Table 1, hydrocarbons are predominantly yielded (up to 68.5%) on Co–ZnAl-LDO/γ-Al_2O_3, with a conversion of 27.0%. The selectivity to ROH is only 29.6%. The introduction of Ga increases the selectivity of alcohols to 61% for a similar conversion (27.3%). This obviously indicates that the presence of Ga promotes CO insertion, which is considered the key step for the formation of alcohols. Also, lower methanol selectivity and higher C_{2+} alcohol fraction in total alcohol products, particularly C_{5+} alcohols, are observed on CoGa–ZnAl-LDO/γ-A_2O_3 than on Co–ZnAl-LDO/γ-Al_2O_3, proving that the introduction of Ga additionally boosts the chain growth probability. Co/ZnGaAl-LDO/γ-A_2O_3 affords lower alcohol selectivity (50.5%) than CoGa–ZnAl-LDO/γ-A_2O_3 (59.8%) for a similar conversion (32.9%). The C_{2+} alcohol fraction is 86.2%. CoGa/ZnAl-LDO/γ-A_2O_3 affords an alcohol selectivity of 51.6%, which is improved in comparison to Co/ZnGaAl-LDO/γ-A_2O_3, while still lower than that on CoGa–ZnAl-LDO/γ-A_2O_3. The C_{2+} alcohol fraction on CoGa/ZnAl-LDO/γ-A_2O_3 (87.3%) is slightly lower than that on CoGa–ZnAl-LDO/γ-A_2O_3 (93.3%). The A–S–F plots of alcohols and hydrocarbons at 15 h are shown in Fig. 7. Accordingly, strictly linear A–S–F distributions are observed for alcohols and hydrocarbons over the entire C_n range for each catalyst. The observation of the correlated α-values is in agreement with a common mechanism of alcohol formation by CO insertion into the same type of intermediate for hydrocarbon formation [24,39]. Obviously, CoGa–ZnAl-LDO/γ-A_2O_3 and CoGa/ZnAl-LDO/γ-A_2O_3 exhibit similarly higher α-values for alcohols and hydrocarbons than the other two catalysts, indicating an enhanced CO insertion ability accompanied by a boosted chain lengthening probability. As resolved from the STEM results, CoGa–ZnAl-LDO/γ-A_2O_3 possesses more contiguous Co and Ga distribution than CoGa/ZnAl-LDO/γ-A_2O_3, and no contiguous distribution of Co and Ga elements has been observed in Co/ZnGaAl-LDO/γ-A_2O_3. Thus it can be concluded that more homogeneous distribution of Co and Ga elements promotes selective formation of not only alcohol products but also C_{2+} alcohols. The intimate contact between Co and Ga sites enhances CO insertion ability and also chain growth probability, making the kinetic rate of CO insertion and C–C coupling match to yield more C_{2+} alcohol products.

In the same reaction time (15 h), CoGa–ZnAl-LDO/γ-A_2O_3 provides higher CO conversion (43.5%) than Co–ZnAl-LDO/γ-A_2O_3 (27.0%), demonstrating the role of Ga in boosting CO conversion.

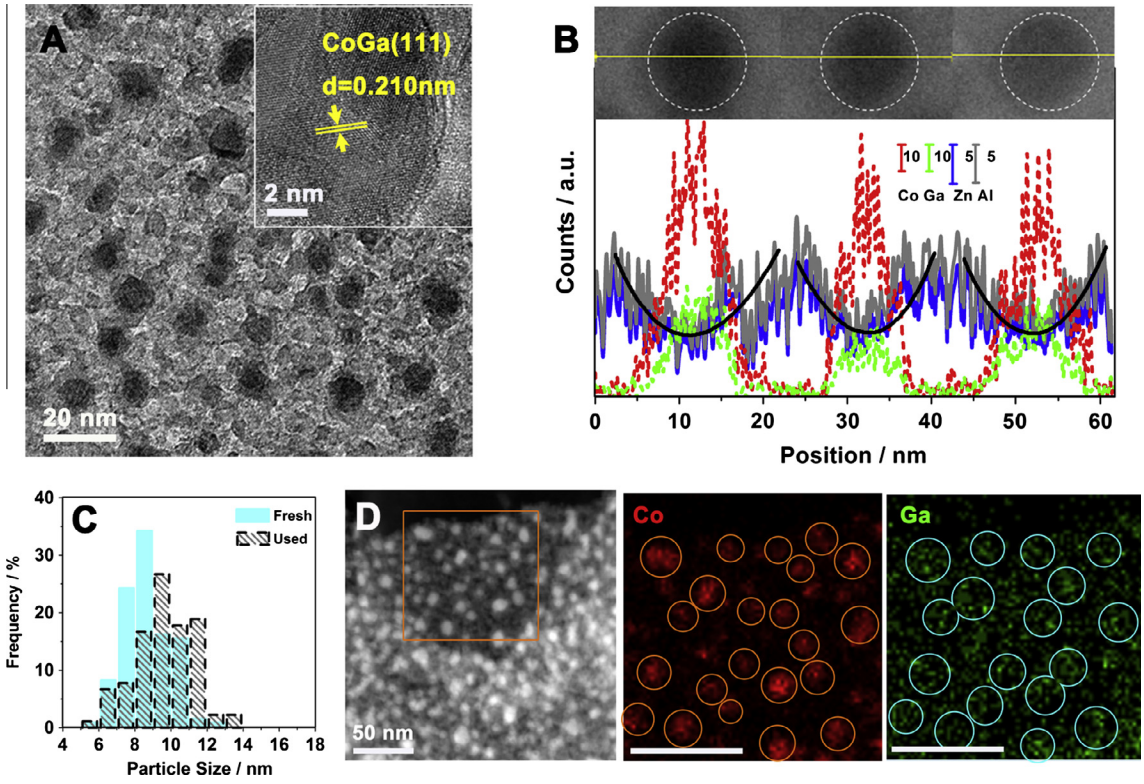

Fig. 10. (A) TEM image with HRTEM image inset and (B) linescan profiles of Co, Ga, Zn, and Al elemental distribution of the used CoGa–ZnAl-LDO/γ-Al_2O_3 after 100 h reaction. (C) The particle size distributions for fresh and used CoGa–ZnAl-LDO/γ-Al_2O_3. (D) HAADF image with the corresponding Co (red) and Ga (green) element mappings in the used CoGa–ZnAl-LDO/γ-Al_2O_3.

CoGa–ZnAl-LDO/γ-A_2O_3, with Co and Ga in homogeneously contiguous distribution, exhibits higher CO conversion than Co/ZnGaAl-LDO/γ-A_2O_3 (32.5%), meaning that CO conversion is also promoted by contiguous Co and Ga distribution. However, CoGa/ZnAl-LDO/γ-A_2O_3 provides much lower CO conversion (15.4%) than CoGa–ZnAl-LDO/γ-A_2O_3 in the same reaction time, although CoGa/ZnAl-LDO/γ-A_2O_3 possesses a contiguous Co and Ga distribution similar to that for CoGa–ZnAl-LDO/γ-A_2O_3. The CO conversion on CoGa/ZnAl-LDO/γ-A_2O_3 is even lower than that on Co/ZnGaAl-LDO/γ-A_2O_3 or Co–ZnAl-LDO/γ-A_2O_3, suggesting that the particle size and size distribution play an important role in determining activity. Smaller particle size leads to higher catalytic activity. Turnover frequencies (TOFs) allow activity comparison without the influence of the particle size, as an earlier study [58] reveals that Co nanoparticles larger than 6 nm have a similar TOF in the Fischer–Tropsch synthesis. As listed in Table 1, the calculated TOF for CoGa–ZnAl-LDO/γ-A_2O_3 is about 37.9×10^{-3} s^{-1}, a little higher than that of the catalyst in the literature [58] under similar experimental conditions ($T = 250$ °C, $P = 3.5$ MPa, TOF = 34.8×10^{-3} s^{-1}). With a similar contiguous Co and Ga distribution, CoGa/ZnAl-LDO/γ-A_2O_3 shows a TOF of 34.2×10^{-3} s^{-1}, which is close to that for CoGa–ZnAl-LDO/γ-A_2O_3. Relatively lower TOFs are obtained on Co–ZnAl-LDO/γ-A_2O_3 (TOF = 29.4×10^{-3} s^{-1}), that is, without Ga, and on Co/ZnGaAl-LDO/γ-A_2O_3 (TOF = 31.8×10^{-3} s^{-1}), that is, without contiguous Co and Ga distribution. It therefore turns out that the activity of Co sites in syngas transformation is boosted by the intimate Ga sites in the well-defined CoGa particles. With CoGa–ZnAl-LDO/γ-A_2O_3 as catalyst, in which Co and Ga are in homogeneously contiguous distribution with CoGa particles narrowly sized between 6 and 14 nm, a CO conversion of 43.5% and an alcohol selectivity of 59%, with a fraction of 93% ethanol and higher alcohols, have been achieved. For comparison, representative catalysts with excellent catalytic performance toward C_{2+} alcohol synthesis from syngas reported in the literature are listed in Table 2. Obviously, the CoGa–ZnAl-LDO/γ-A_2O_3 catalyst turns into one of the catalysts having the potential for scale-up in an industrial application to produce ethanol and higher alcohols, owing to the high selectivity to alcohols or C_{2+} alcohols with a relatively high CO conversion.

For further study, reactions at different temperatures on CoGa–ZnAl-LDO/γ-A_2O_3 and Co/ZnGaAl-LDO/γ-A_2O_3 were carried out. Fig. 8 illustrates CO conversion as a function of reaction temperature, as well as the selectivity to alcohols and fraction to C_{2+} alcohols versus CO conversion. Generally, increasing reaction temperature results in a continuous increase in catalytic activity, while CoGa–ZnAl-LDO/γ-A_2O_3 shows higher conversion than Co/ZnGaAl-LDO/γ-A_2O_3 at each temperature. A CO conversion of 40% is obtained at 256 °C on CoGa–ZnAl-LDO/γ-A_2O_3, while 280 °C is required on Co/ZnGaAl-LDO/γ-A_2O_3 to reach the same conversion (Fig. 8A). In the case of CoGa–ZnAl-LDO/γ-A_2O_3, the selectivity to alcohols reaches 63%, and 93% of the total alcohols is C_{2+} alcohols (Fig. 8B) at 40% conversion. But in the case of Co/ZnGaAl-LDO/γ-A_2O_3, the selectivity to alcohols and the fraction of C_{2+} alcohols are only 38% and 79%. The results further suggest that the uniform Co and Ga dispersion of the CoZnGaAl-LDHs/γ-Al_2O_3 precursor improves the selective production of ethanol and higher alcohols from syngas.

These results demonstrate that the presence of Ga in the CoGa catalyst enhances both the activity and alcohol selectivity in ethanol and higher alcohol synthesis from syngas, which can be preliminarily understood in the following two ways. First, the doping of Ga with contiguous distribution of Co contributes to isolating more Co centers, on which associative CO adsorption is favored. Thus, the associative CO insertion step is accelerated on CoGa–ZnAl-LDO/γ-A_2O_3, increasing the selectivity of alcohols. Second, the intimate contact of Co and Ga in the well-defined CoGa

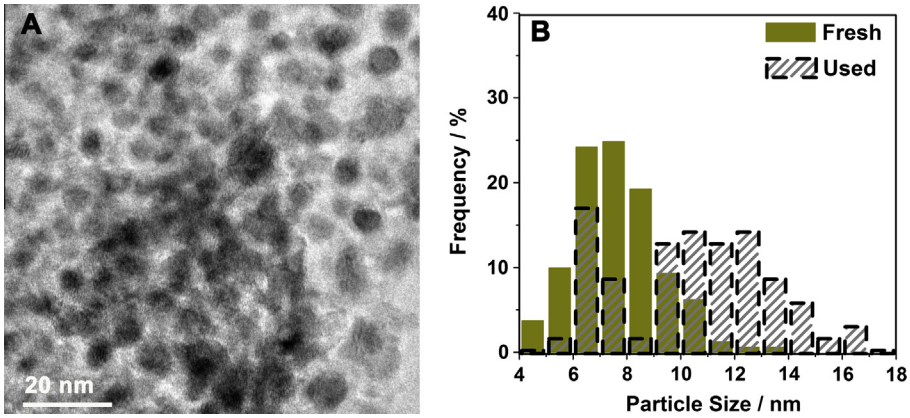

Fig. 11. (A) TEM image of the used Co/ZnGaAl-LDO/γ-Al_2O_3 after 100 h reaction. (B) The particle size distributions for fresh and used Co/ZnGaAl-LDO/γ-Al_2O_3.

particles facilitates electron transfer from Ga to Co. The adjacent electron-rich Co centers are efficient for CO dissociative adsorption and the subsequent C–C coupling, which enhances the CO conversion/surface activity and the carbon chain growth. The unique structural features of CoGa catalysts need further investigation for the understanding of the role of Ga in the catalysis, which is under way in our laboratory.

3.2.2. Enhanced stability of trapped CoGa catalyst

The stability of CoGa–ZnAl-LDO/γ-Al_2O_3 and Co/ZnGaAl-LDO/γ-Al_2O_3 was tested under medium reaction conditions for over 100 h. The conversion of CO and the selectivity to alcohols as a function of time on stream are presented in Fig. 9. After an initial induction period, the CO conversion and ROH selectivity remain stable at approximately 43% and 60% on CoGa–ZnAl-LDO/γ-Al_2O_3. By contrast, on Co/ZnGaAl-LDO/γ-Al_2O_3, the CO conversion begins to decrease after 40 h and gradually attains stabilization at a lower activity of 20%. The selectivity to ROH also drops nearly to 40%, following the loss of activity. The stable catalysis of CoGa–ZnAl-LDO/γ-Al_2O_3 is assumed to result from the trapping effects of ZnAl-LDO on CoGa particles. As can be seen in the TEM image (Fig. 10A) and the linescan profiles of each elemental population (Fig. 10B) of the used CoGa–ZnAl-LDO/γ-Al_2O_3, the trapped CoGa particles are still clearly observed. No obvious aggregation is observed with CoGa particles between 6 and 14 nm (mean size 9.6 nm, Fig. 10C). The Co and Ga retain a contiguous distribution even after a long-term reaction (Fig. 10B and D). But for used Co/ZnGaAl-LDO/γ-Al_2O_3, the aggregation of the particles can be clearly observed due to the lack of the confined effect of the LDO support (Fig. 11A). Most of the particles increase to 9–17 nm (Fig. 11B), which accounts for the decrease in catalytic activity after 40 h.

4. Conclusions

In summary, this work proposes a uniformly dispersed CoGa catalyst for ethanol and higher alcohols synthesis from syngas, with the CoGa particles trapped in the oxide. The well-defined CoGa particles with a narrow size distribution, as well as the trapped structure, have been produced from the reduction of CoGaZnAl-LDHs/γ-Al_2O_3. This CoGa catalyst provides a CO conversion of 43.5% with a selectivity of 59% to alcohols. Among the alcohol products, the fraction of ethanol and higher alcohols reaches 93%. More significantly, the trapped CoGa shows no visible changes of particle dispersion and homogeneous CoGa distribution in the reaction, which gives rise to stable catalytic performance. Further study of the promoting nature of the Ga component is going on in our laboratory.

Acknowledgments

Financial support by National Nature Science Foundation of China (NSFC), PCSIRT (IRT1205), the 973 Project (2011CBA00504, 2014CB932101), and the Fundamental Research Funds for the Central Universities (YS1406) is gratefully acknowledged. J.H. particularly appreciates the financial aid of the China National Funds for Distinguished Young Scientists from the NSFC. This work is also supported by the Beijing Engineering Center for Hierarchical Catalysts.

Appendix A. Supplementary material

Supplementary data associated with this article can be found, in the online version, at http://dx.doi.org/10.1016/j.jcat.2016.05.014.

References

[1] P. Forzatti, E. Tronconi, I. Pasquon, Chem. Rev. 33 (1991) 109.
[2] R. Herman, Catal. Today 55 (2000) 233.
[3] J.J. Spivey, A. Egbebi, Chem. Soc. Rev. 36 (2007) 1514.
[4] V. Subramani, S.K. Gangwal, Energy Fuels 22 (2008) 814.
[5] K. Fang, D. Li, M. Lin, M. Xiang, W. Wei, Y. Sun, Catal. Today 147 (2009) 133.
[6] M. Gupta, M.L. Smith, J.J. Spivey, ACS Catal. 1 (2011) 641.
[7] V.R. Surisetty, A.K. Dalai, J. Kozinski, Appl. Catal. A 404 (2011) 1.
[8] K. Kon, S.M.A. Hakim Siddiki, K.-I. Shimizu, J. Catal. 304 (2013) 63.
[9] S. Roy, G. Mpourmpakis, D.-Y. Hong, D.G. Vlachos, A. Bhan, R.J. Gorte, ACS Catal. 2 (2012) 1846.
[10] S.J. Yoon, J. Goo Lee, Energy Fuels 26 (2012) 524.
[11] Q. Guo, Y. Cheng, Y. Liu, W. Jia, H.-J. Ryu, Ind. Eng. Chem. Res. 53 (2014) 78.
[12] L.J.L. Maciel, S.M.D. Vasconcelos, A. Knoechelmann, C.A.M.D. Abreu, Stud. Surf. Sci. Catal. 167 (2007) 469.
[13] A. Sunny, P.A. Solomon, K. Aparna, J. Nat. Gas Sci. Eng. 30 (2016) 176.
[14] B.G. Bryan, A. Basu, H.S. Meyer, U.S. Patent 0299589, 2015.
[15] M.M. Yung, W.S. Jablonski, K.A. Magrinibair, Energy Fuels 23 (2009) 1874.
[16] R. Rauch, J. Hrbek, H. Hofbauer, Wiley Interdiscipl. Rev. Energy Environ. 3 (2014) 343.
[17] J. Cheng, P. Hu, P. Ellis, S. French, G. Kelly, C.M. Lok, J. Phys. Chem. C 112 (2008) 9464.
[18] J. Wang, X. Zhang, Q. Sun, S. Chan, H. Su, Catal. Commun. 61 (2015) 57.
[19] X. Pan, Z. Fan, W. Chen, Y. Ding, H. Luo, X. Bao, Nat. Mater. 6 (2007) 507.
[20] Z. Fan, W. Chen, X. Pan, X. Bao, Catal. Today 147 (2009) 86.
[21] Y. Huang, W. Deng, E. Guo, P.-W. Chung, S. Chen, B.G. Trewyn, R.C. Brown, V.S. Y. Lin, ChemCatChem 4 (2012) 674.
[22] W. Gao, Y. Zhao, J. Liu, Q. Huang, S. He, C. Li, J. Zhao, M. Wei, Catal. Sci. Technol. 3 (2013) 1324.
[23] Z. Bao, K. Xiao, X. Qi, X. Wang, L. Zhong, K. Fang, M. Lin, Y. Sun, J. Energy Chem. 22 (2013) 107.
[24] Y. Lu, B. Cao, F. Yu, J. Liu, Z. Bao, J. Gao, ChemCatChem 6 (2014) 473.
[25] S. Zaman, K.J. Smith, Chem. Rev. 54 (2012) 41.

[26] Q. Wu, J.M. Christensen, G.L. Chiarello, L.D. Duchstein, J.B. Wagner, B. Temel, J.-D. Grunwaldt, A.D. Jensen, Catal. Today 215 (2013) 162.
[27] E.T. Liakakou, E. Heracleous, K.S. Triantafyllidis, A.A. Lemonidou, Appl. Catal. B 165 (2015) 296.
[28] A.Y. Khodakov, C. Wei, F. Pascal, Chem. Rev. 38 (2007) 1692.
[29] A. Venugopal, J. Aluha, M.S. Scurrell, Catal. Lett. 90 (2003) 1.
[30] A.K. Dalai, B.H. Davis, Appl. Catal. A 348 (2008) 1.
[31] N. Kumar, M.L. Smith, J.J. Spivey, J. Catal. 289 (2012) 218.
[32] J. Anton, J. Nebel, H. Song, C. Froese, P. Weide, H. Ruland, M. Muhler, S. Kaluza, J. Catal. 335 (2016) 175.
[33] Y.Z. Fang, Y. Liu, L.H. Zhang, Appl. Catal. A 397 (2011) 183.
[34] J. Wang, P.A. Chernavskii, A.Y. Khodakov, Y. Wang, J. Catal. 286 (2012) 51.
[35] Y. Xiang, V. Chitry, P. Liddicoat, P. Felfer, J. Cairney, S. Ringer, N. Kruse, J. Am. Chem. Soc. 135 (2013) 7114.
[36] G. Prieto, S. Beijer, M.L. Smith, M. He, Y. Au, Z. Wang, D.A. Bruce, K.P. de Jong, J.J. Spivey, P.E. de Jongh, Angew. Chem. Int. Ed. 53 (2014) 6397.
[37] W. Gao, Y. Zhao, H. Chen, H. Chen, Y. Li, S. He, Y. Zhang, M. Wei, D.G. Evans, X. Duan, Green Chem. 17 (2015) 1525.
[38] Y. Xiang, R. Barbosa, X. Li, N. Kruse, ACS Catal. 5 (2015) 2929.
[39] G. Jiao, Y. Ding, H. Zhu, X. Li, J. Li, R. Lin, W. Dong, L. Gong, Y. Pei, Y. Lu, Appl. Catal. A 364 (2009) 137.
[40] V.M. Lebarbier, D. Mei, D.H. Kim, A. Andersen, J.L. Male, J.E. Holladay, R. Rousseau, Y. Wang, J. Phys. Chem. C 115 (2011) 17440.
[41] Y.-P. Pei, J.-X. Liu, Y.-H. Zhao, Y.-J. Ding, T. Liu, W.-D. Dong, H.-J. Zhu, H.-Y. Su, L. Yan, J.-L. Li, ACS Catal. 5 (2015) 3620.
[42] G.-L. Liu, T. Niu, A. Cao, Y.-X. Geng, Y. Zhang, Y. Liu, Fuel 176 (2016) 1.
[43] Y. Yang, X. Qi, X. Wang, L. Dong, Y. Fei, L. Zhong, W. Hui, Y. Sun, Catal. Today 270 (2015) 101.
[44] S. Carenco, A. Tuxen, M. Chintapalli, E. Pach, C. Escudero, T.D. Ewers, P. Jiang, F. Borondics, G. Thornton, A.P. Alivisatos, H. Bluhm, J. Guo, M. Salmeron, J. Phys. Chem. C 117 (2013) 6259.
[45] K. Xiao, Z. Bao, X. Qi, X. Wang, L. Zhong, K. Fang, M. Lin, Y. Sun, J. Mol. Catal. A: Chem. 378 (2013) 319.
[46] N. Tien-Thao, M.H. Zahedi-Niaki, H. Alamdari, S. Kaliaguine, Appl. Catal. A 326 (2007) 152.
[47] P.J. Sideris, U.G. Nielsen, Z. Gan, C.P. Grey, Science 321 (2008) 113.
[48] M.-Q. Zhao, Q. Zhang, W. Zhang, J.-Q. Huang, Y. Zhang, D.S. Su, F. Wei, J. Am. Chem. Soc. 132 (2010) 14739.
[49] L. He, Y. Huang, A. Wang, X. Wang, X. Chen, J.J. Delgado, T. Zhang, Angew. Chem. 51 (2012) 6191.
[50] S. He, C. Li, H. Chen, D. Su, B. Zhang, X. Cao, B. Wang, M. Wei, D.G. Evans, X. Duan, Chem. Mater. 25 (2013) 1040.
[51] Y. He, L. Liang, Y. Liu, J. Feng, C. Ma, D. Li, J. Catal. 309 (2014) 166.
[52] J.-T. Feng, Y.-J. Lin, D.G. Evans, X. Duan, D.-Q. Li, J. Catal. 266 (2009) 351.
[53] G.R. Johnson, A.T. Bell, J. Catal. 338 (2016) 250.
[54] C. Gennequin, S. Siffert, R. Cousin, A. Aboukaïs, Top. Catal. 52 (2009) 482.
[55] N. Al-Yassir, M.N. Akhtar, S. Al-Khattaf, J. Por. Mater. 19 (2011) 943.
[56] S. Oyama, X. Zhang, J. Lu, Y. Gu, T. Fujitani, J. Catal. 257 (2008) 1.
[57] Y. He, Y. Liu, P. Yang, Y. Du, J. Feng, X. Cao, J. Yang, D. Li, J. Catal. 330 (2015) 61.
[58] G.L. Bezemer, J.H. Bitter, H.P. Kuipers, H. Oosterbeek, J.E. Holewijn, X. Xu, F. Kapteijn, A.J. van Dillen, K.P. de Jong, J. Am. Chem. Soc. 128 (2006) 3956.
[59] G. Liu, T. Niu, D. Pan, F. Liu, Y. Liu, Appl. Catal. A 483 (2014) 10.